# Inhibition of calcium carbonate crystal growth by organic additives using the constant composition method in conditions of recirculating cooling circuits

Norinda Chhim, Chams Kharbachi, Thibaut Neveux, Céline Bouteleux, Sébastien Teychené, Béatrice Biscans

# Inhibition of calcium carbonate crystal growth by organic additives using the constant composition method in conditions of recirculating cooling circuits

Norinda Chhim [a,b], Chams Kharbachi [b], Thibaut Neveux [a], Céline Bouteleux [a], Sébastien Teychené [b], Béatrice Biscans [b,*]

[a] EDF Lab Chatou, 6 quai Watier, 78401 Chatou Cedex, France
[b] Laboratoire de Génie Chimique, Université de Toulouse, CNRS, INPT, UPS, 4 allée Emile Monso CS84234, 31432 Toulouse, France

*Keywords:*
A1. Precipitation
A1. Constant supersaturation ratio
A1. Scaling
A1. Additives
B1. Calcium carbonate

A B S T R A C T

The cooling circuits used in power plants are subject to mineral crystallization which can cause scaling on the surfaces of equipment and construction materials reducing their heat exchange efficiency. Precipitated calcium carbonate is the predominant mineral scale commonly observed in cooling systems. Supersaturation is the key parameter controlling the nucleation and growth of calcite in these systems. The present work focuses on the precipitation of calcite using the constant composition method at constant supersaturation, through controlled addition of reactants to a semi-batch crystallizer, in order to maintain constant solution pH. The determination of the thermodynamic driving force (supersaturation) was based on the relevant chemical equilibria, total alkalinity and calculation of the activity coefficients. Calcite crystallization rates were derived from the experiments performed at supersaturation levels similar to those found in industrial station cooling circuits. Several types of seeds particles were added into the aqueous solution to mimic natural river water conditions in terms of suspended particulate matters content, typically: calcite, silica or illite particles. The effect of citric and copolycarboxylic additive inhibitors added to the aqueous solution was studied. The calcium carbonate growth rate was reduced by 38.6% in the presence of the citric additive and a reduction of 92.7% was observed when the copolycarboxylic additive was used under identical experimental conditions. These results are explained by the location of the adsorbed inhibitor at the crystal surface and by the degree of chemical bonding to the surface.

## 1. Introduction

Mineral crystallization fouling and deposition of mineral particles such as calcium carbonate ($CaCO_3$), associated with the presence of suspended matters in cooling water, occur on the surfaces of cooling circuits and can lead to the formation of hard scale layers, which increase heat transfer resistance, and consequently reduce heat exchange efficiency. This is a major issue in industrial production, particularly in energy-intensive operations, such as thermal and nuclear power plants cooling systems [1,2], membrane desalination and reverse osmosis [3,4], distillation [5,6] and oilfield production processes [7]. In these processes, $CaCO_3$ precipitation and/or deposition is due to the evaporation of water in cooling towers resulting in higher concentrations of dissolved salts (especially calcium and bicarbonate) and also of suspended matters. Increases in these concentrations alter chemical equilibria, inducing the crystallization of dissolved substances and scale deposition on heat exchange equipment surfaces. Furthermore, increases in water temperature promote calcium carbonate precipitation both kinetically (increase of reaction kinetics) and thermodynamically (decreased solubility).

Fouling and/or scale deposition can cause technical problems, such as reduced heat transfer efficiency and partial or total clogging of condenser tubes and pipes. Economically, the preventive and control actions necessitated by these technical problems can also increase operational costs. In addition, structures are weakened, requiring considerable maintenance, hence reducing the lifespan of equipment. The non-productive expense associated with scaling is estimated at 1.5 billion Euros per year in France, the equivalent of around 0.8 billion $ US in Great Britain, 3 billion $US in Japan and 9 billion $ in the USA [8].

* Corresponding author.
*E-mail address:* beatrice.biscans@ensiacet.fr (B. Biscans).

http://dx.doi.org/10.1016/j.jcrysgro.2017.03.004

Numerous studies on fundamental phenomena involved in precipitation [9], crystallization [10], crystal growth [11,12] and calcium carbonate aggregation [13] have demonstrated the significance of the supersaturation level [14,15]. The solution composition [16,17], pH [18,19], temperature [20], as well as the presence of seeds [21,22] and foreign substances such as dissolved organic matter [23,24], $Mg^{2+}$ ions [25,26] or $Cu^{2+}$ and $Zn^{2+}$ ions [27,28] have been previously studied and shown to affect these phenomena.

The constant composition method is suitable for the study of crystallization processes at constant supersaturation [29,24]. To our knowledge, very few studies have been carried out with the use of constant composition for calcium carbonate crystallization in a large capacity reactor.

In this study, the emphasis is placed on the transposition of the constant composition method for crystallization of calcium carbonate to the precipitation of calcite, in order to replicate experimentally the operating conditions of recirculating cooling water systems, especially with respect to the supersaturation range, presence of suspended matters (such as illite, silica, calcite) and temperature range encountered, as well as the polymeric scale inhibitors used in these circuits.

## 2. Theoretical calculations

### 2.1. Chemical equilibria

#### 2.1.1. Equilibrium constants

In this work, calcium carbonate seed crystals are grown in supersaturated solution. In order to compensate the depletion of calcium and carbonate in the reactor resulting from the calcium carbonate crystal growth, two reactants are added progressively in the reactor: calcium chloride $CaCl_2$ solution (reactant 1) and sodium carbonate $Na_2CO_3$ solution (reactant 2). A preliminary calculation of the supersaturation ratio is performed based on the chemical equilibria and activity coefficients of the species involved.

The relation between the activity $a_j$ and the free concentration $c_j$ (mol/L) is given by Eq. (1):

$$a_j = \gamma_j c_j \tag{1}$$

with $\gamma_j$ the activity coefficient, where $\gamma_j$ tends to 1 when the solute concentration $c_j$ tends to zero (infinite dilution), and $\gamma_{water}$ tends to 1 when the mole fraction of water tends to one (asymmetric convention). The activity (effective free concentrations) of compounds present in a system at equilibrium conditions are related together by the thermodynamic equilibrium constants $K_j$ which are temperature dependent. The equilibrium constant for the autoprotolysis of water, $K_w$, is given by the product of the activity of the hydroxide ions, $a_{OH^-}$, and the protons ($H^+$ ions), $a_{H^+}$:

$$K_{water} = a_{OH^-} a_{H^+} \tag{2}$$

and the pH of the solution by:

$$pH = -\log(a_{H^+}) \tag{3}$$

The $HCO_3^- \Leftrightarrow CO_3^{2-} + H^+$ equilibrium is described by:

$$K_{HCO_3^-} = \frac{a_{CO_3^{2-}} a_{H^+}}{a_{HCO_3^-}} \tag{4}$$

The equilibrium constant $K_{CO2}$ determines the extent of the reactions between $HCO_3^-$, $H^+$, dissolved $CO_2$ and $H_2O$ in the solution:

$$CO_{2(aq)} + H_2O \Longleftrightarrow HCO_3^- + H^+ \quad K_{CO_2} = \frac{a_{HCO_3^-} a_{H^+}}{a_{CO_{2(aq)}}} \tag{5}$$

The activity of $CO_2$ (aq) shown in Eq. (5) is given by Henry's Law which describes the thermodynamic equilibrium between atmospheric (gaseous) $CO_2$ and dissolved $CO_2$ (6):

$$CO_{2(g)} \Longleftrightarrow CO_{2(aq)} \quad H_{CO_2} = \frac{a_{CO_{2(aq)}}}{p_{CO_2}} \tag{6}$$

where $H_{CO2}$ is the Henry's Law constant, expressed in mol/(L atm) and the term $p_{CO2}$ represents the partial pressure of the $CO_2$ above the solution expressed in atm. The value of the Henry's constant depends on the temperature. The partial ion-pair association of calcium, bicarbonate and carbonate ions in the aqueous phase leads to the formation of $CaCO_3^0$(aq), and $CaHCO_3^+$ complexes.

$$Ca^{2+} + CO_3^{2-} \Longleftrightarrow CaCO_3^0(aq) \quad K_{CaCO_3^0} = \frac{a_{CaCO_3^0}}{a_{Ca^{2+}} a_{CO_3^{2-}}} \tag{7}$$

$$Ca^{2+} + HCO_3^- \Longleftrightarrow CaHCO_3^+ \quad K_{CaHCO_3^+} = \frac{a_{CaHCO_3^+}}{a_{Ca^{2+}} a_{HCO_3^-}} \tag{8}$$

#### 2.1.2. Total calcium concentration and total alkalinity

The condition of electrical neutrality in the working solution is given by the following equation:

$$2C_{Ca}^{2+} + C_{CaHCO3}^{+} + C_{H}^{+} + C_{Na}^{+} = 2C_{CO3}^{2-} + C_{HCO3}^{-} + C_{OH}^{-} + C_{Cl}^{-} \tag{9}$$

and the total calcium concentration by:

$$C_{Ca,total} = C_{Ca}^{2+} + C_{CaHCO3}^{+} + C_{CaCO3^0(aq)} \tag{10}$$

The expression of the free calcium concentration $C_{Ca2+}$ in Eq. (10) can be substituted into Eq. (9), which is then rearranged into pH dependent species (right hand side) and pH independent species (left hand side) to obtain Eq. (11), assuming that complexation with sodium ions is negligible.

$$C_{Na+} - C_{Cl-} + 2C_{Ca,total} = 2C_{CO3}^{2-} + C_{HCO3}^{-} + C_{OH}^{-} - C_{H}^{+} + C_{CaHCO3}^{+} + 2C_{CaCO3^0(aq)} \tag{11}$$

The right hand side represents the sum of all the titratable bases and is defined as the total alkalinity of the working solution $C_{alk,total}$:

$$C_{alk,total} = 2C_{CO3}^{2-} + C_{HCO3}^{-} + C_{OH}^{-} - C_{H+} + C_{CaHCO3}^{+} + 2C_{CaCO3^0(aq)} \tag{12}$$

#### 2.1.3. Ionic strength and activity coefficients of the working solution

The activity coefficient of the ion j can be calculated either from the Debye-Hückel model when the ionic strength is I < 0.1 M or by using the Davies (13) equation where the ionic strength is I < 0.5 M and is defined by the following law:

$$\log \gamma_j = -Az_j^2 \left( \frac{\sqrt{I}}{1+\sqrt{I}} - 0.3I \right) \tag{13}$$

wherein $z_j$ denotes the valence of ion j, and A is the Debye-Hückel constant (a function of temperature, with A = 0.509 at 25 °C). The ionic strength I is expressed in $mol{\cdot}L^{-1}$ and is defined, for j ions in the working solution, by:

$$I = \sum_j \frac{1}{2} C_j z_j^2 \tag{14}$$

The total ionic strength of the solution in the precipitation reactor is expressed in mol/L and is calculated based on the following concentration ratios:

$$I = \frac{1}{2}(C_{H+} + C_{OH-} + 4C_{CO32-} + C_{HCO3-} + 4C_{Ca2+} + C_{CaHCO3+} + C_{Na+} + C_{Cl-}) \tag{15}$$

### 2.2. Supersaturation ratio calculation

The values of the equilibrium constants $K_j$ and the theoretical values of the Henry's Law constant described in Section 2.1 are reported in Table 1A for the operating temperature range encountered in industrial recirculating cooling circuits. In this work, we have calculated the $\log K_s$ values (Ks is the solubility product, which is the equilibrium constant for a solid substance dissolving in an aqueous solution) for calcite at different temperatures (25–45 °C) using Eq. (16), derived from Plummer and Busenberg [30] work:

$$\log K_s = -171.9065 - 0.077993(273.15 + \theta) + 2839.319/(273.15 + \theta) + 71.595 \log(273.15 + \theta) \quad (16)$$

where θ is the temperature of the working solution expressed in °C.

The supersaturation ratio Ω for calcium carbonate is defined by the classical equation:

$$\Omega = \frac{a_{Ca^{2+}} \cdot a_{CO_3^{2-}}}{K_s} \quad (17)$$

where $a_{Ca^{2+}}$ and $a_{CO_3^{2-}}$ represent respectively the activity of $Ca^{2+}$ and $CO_3^{2-}$ ions and $K_s$ is the calcium carbonate solubility product (calcite, in our case) at the working temperature. The supersaturation Ω, activity of the $Ca^{2+}$ and $CO_3^{2-}$ ions, ionic strength I, total alkalinity and concentrations of the species present in the solution are calculated using the PHREEQC software [31] developed by the US Geological Survey, which also allows to calculate the speciation of different species as a function of supersaturation for a range of supersaturation ratios.

For each temperature, the initial composition of the working solution is calculated by iteration until $\log\left(\frac{a_{Ca^{2+}} \cdot a_{CO_3^{2-}}}{K_s}\right)$ reaches the desired value for the preliminary fixed supersaturation ratio ($\log\Omega$). However, in our system, the pH and the ionic strength of the solution are difficult to maintain constant and vary with increasing supersaturation ratio. To stabilize these parameters, it was decided to add sodium chloride (NaCl) into the solution. The compositions of the initial solution at 25 °C, including the NaCl concentration for each supersaturation ratio, obtained from PHREEQC simulations are reported in Table 1B. Identical calculations (not reported here) were made for the other two working temperatures (35 °C, 45 °C).

The first step in the experimental work consists in understanding the carbon dioxide exchange with the ambient air above the thermostated reactor. Indeed, the exchange of $CO_2$ present in the

**Table 1**
Equilibrium constants [58,30]. (A) and composition of the working solution in the presence of NaCl to maintain stability of pH and ionic strength, simulated with the PHREEQC software, at 25 °C (B).

| Equilibrium constants | 25 °C | 35 °C | 45 °C |
|---|---|---|---|
| *(A)* | | | |
| $K_{water}$ $(mol{\cdot}L^{-1})^2$ | $1.01 \cdot 10^{-14}$ | $2.07 \cdot 10^{-14}$ | $3.94 \cdot 10^{-14}$ |
| $K_{HCO_3^-}$ $(mol{\cdot}L^{-1})$ | $4.69 \cdot 10^{-11}$ | $5.60 \cdot 10^{-11}$ | $6.37 \cdot 10^{-11}$ |
| $K_{CO_2}$ $(mol{\cdot}L^{-1})$ | $4.45 \cdot 10^{-7}$ | $4.90 \cdot 10^{-7}$ | $5.14 \cdot 10^{-7}$ |
| $H_{CO_2}$ $(mol{\cdot}L^{-1}{\cdot}atm)$ | $3.40 \cdot 10^{-2}$ | $2.65 \cdot 10^{-2}$ | $2.14 \cdot 10^{-2}$ |
| $K_{CaCO_3^0}$ $(mol{\cdot}L^{-1})^{-1}$ | $1.66 \cdot 10^{3}$ | $2.11 \cdot 10^{3}$ | $2.79 \cdot 10^{3}$ |
| $K_{CaHCO_3^+}$ $(mol{\cdot}L^{-1})^{-1}$ | $1.28 \cdot 10^{1}$ | $1.44 \cdot 10^{1}$ | $1.56 \cdot 10^{1}$ |

| Ω | 5 | 7.6 | 15 | 35 | 50 |
|---|---|---|---|---|---|
| *(B)* | | | | | |
| $\log\Omega$ | 0.7 | 0.88 | 1.179 | 1.546 | 1.698 |
| $Na_2CO_3$ $(mol{\cdot}L^{-1})$ | 0.00725 | 0.00725 | 0.013 | 0.022 | 0.0265 |
| $CaCl_2$ $(mol{\cdot}L^{-1})$ | 0.00725 | 0.00725 | 0.013 | 0.022 | 0.0265 |
| NaCl $(mol{\cdot}L^{-1})$ | 0.1 | 0.1 | 0.08 | 0.04 | 0.01 |
| pH | 8.06 | 8.5 | 8.02 | 7.999 | 7.995 |
| I $(mol{\cdot}L^{-1})$ | $4.25 \cdot 10^{-2}$ | $4.26 \cdot 10^{-2}$ | $4.25 \cdot 10^{-2}$ | $4.29 \cdot 10^{-2}$ | $4.20 \cdot 10^{-2}$ |

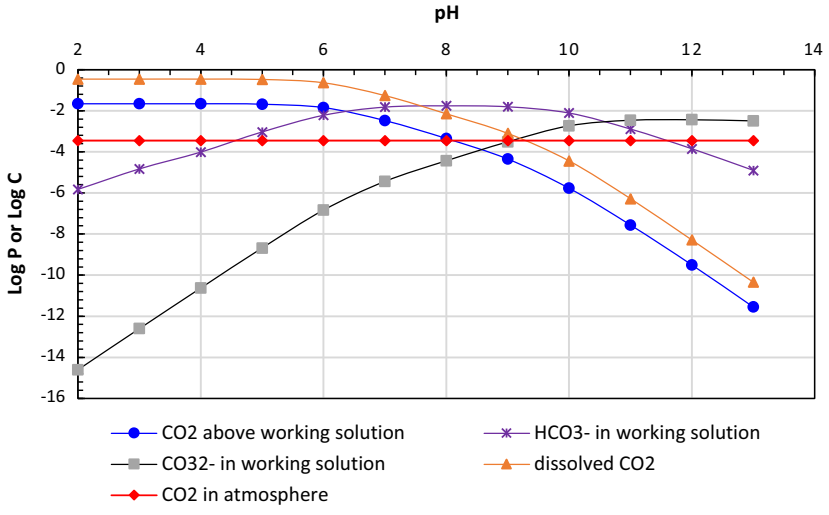


**Fig. 1.** Evolution of the partial pressures and concentrations of the species of interest at 25 °C.

air with the working solution during experiments could lead to variations in the concentration of carbon species in the reactor. A new simulation was performed, varying the solution pH in order to assess its effect on the absorption and desorption of $CO_2$ in the working solution. The interest parameters obtained from PHREEQC simulation are the partial pressure of $CO_2$ above the working solution, the partial pressure of $CO_2$ in the atmosphere, the dissolved $CO_2$ concentration and the concentrations of $CO_3^{2-}$ and $HCO_3^-$ ions. The values of these parameters for the working solution at 25 °C containing 0.065 mol of $Na_2CO_3$, 0.009 mol of $CaCl_2$ and 0.04 mol of NaCl are shown in Fig. 1. Moreover, the concentrations of the different species of interest calculated using the PHREEQC program must satisfy both the equation of electrical neutrality (9) and the equation giving the total concentration of carbon species in the working solution:

$$C_{C,total} = C_{CO_2(aq)} + C_{CO_3^{2-}} + C_{HCO_3^-} + C_{CaHCO_3^+} + C_{CaCO_3^0(aq)} \quad (18)$$

The partial pressure of the $CO_2$ above the working solution and the concentration of dissolved $CO_2$ both decrease with increasing pH. Furthermore, the partial pressure of $CO_2$ above the solution is relatively close to the atmospheric pressure of $CO_2$ in the pH range from 8.0 to 8.5 ($\Delta p_{CO2} = -2.1 \cdot 10^{-4}$ atm at pH = 8.5), which corresponds to the values typically encountered in recirculating cooling water systems. As this will be the working pH range for the experiments, the use of a nitrogen sweep gas in the space above the solution will not be necessary.

These results enable us to control the process of $CO_2$ absorption into the solution and the associated decrease in the solution pH which might otherwise interfere with the pH variation due to precipitation of calcium carbonate and could in turn lead to the overestimation of the crystal growth rate.

## 3. Experimental methods

### 3.1. Experimental set-up

Using the constant composition method, an initial supersaturated solution was prepared by mixing a solution of calcium chloride dihydrate (purity 99–105% Panreac, ref. 141232.1210) and anhydrous sodium carbonate (99.95–100.05% purity, Sigma-Aldrich, ref. 223484) in a stirred reactor. Sodium chloride, analytical grade, was also added to the solution in order to maintain a constant ionic strength. The working solution was stable for periods exceeding 24 h and was supersaturated with respect to all calcium carbonate polymorphs. All experiments were conducted in a 1000 mL double walled jacketed glass reactor equipped with a PTFE propeller and 4 baffles, working at a stirring rate of 100 rpm. The temperature within the reactor was kept constant by means of thermostat circulating water. Pre-calibrated calcite seed crystals (99% pure, Merck, ref. 1.02066) were introduced into the reactor. Various probes (temperature sensor, pH electrode, conductivity sensor, $Ca^{2+}$ electrode) were immersed in the reactor. The reactor was tightly sealed during the experiments to minimize an air-gas exchange with surrounding room air. Two reactant solutions ($Ca^{2+}$ and $CO_3^{2-}$), connected to 905 Titrando (Metrohm) burettes and the Tiamo 2.5 remote control software, were used to compensate pH decreases resulting from the depletion of $Ca^{2+}$ and $CO_3^{2-}$ in the working solution due to the $CaCO_3$ precipitation reaction. They are added with the same flowrate. The pH was kept constant in the reactor by simultaneously adding measured volumes of the two reactant solutions. The injected volume of each reactant solution and the pH in the reactor were recorded over time to allow determination of the growth kinetics of the calcite seed crystals introduced into the supersaturated solution. A schematic illustration of the experimental setup used for all constant composition tests is shown in Fig. 2.

The concentrations of reacting solutions were optimized to 12 times more concentrate than the working solution in the reactor to avoid excessive increase in the working volume (generally limited to less than 5%) over the course of the test.

For example, the composition of the working solution at supersaturation ratio $\Omega = 5$ is $7.25 \cdot 10^{-3}$ M of $Na_2CO_3$, $7.25 \cdot 10^{-3}$ M of $CaCl_2$ + 0.1 M of NaCl (see Table 1B) and the corresponding compositions of the reactant solutions are:

Reactant 1: $8.7 \cdot 10^{-2}$ M of $CaCl_2$ + 0.6 M of NaCl.
Reactant 2: $8.7 \cdot 10^{-2}$ M of $Na_2CO_3$ + 0.6 M of NaCl.

In the experiments with inhibitors, the additive is added directly into the working solution to reach a 0.5 mg·L$^{-1}$ concentration of active ingredient. The pH of the working solution is adjusted to 8.5 either with 1 M hydrochloric acid or with 1 M sodium hydroxide depending on the value measured in the working solution. The solution conductivity and $Ca^{2+}$ concentration are continuously monitored. In addition, at the end of each experiment, the free $Ca^{2+}$ concentration is determined by EDTA titration, after membrane filtration (Millipore 0.2 μm), in order to verify that the calcium concentration remained constant throughout the crystallization experiment.

### 3.2. Seed and additive characteristics

Several types of particles are found in river water passing through cooling systems, mainly calcite, silica and/or illite, all three of which were used as seed particles in our experiments. Table 2A reports the average particle size and specific surface area of each seed type. The characteristics of the two additives used in the experiments to inhibit calcite growth or aggregation are summarized in Table 2C.

The choice of these three mineral particles as « model » seeds in all of our experiments is based on the results of mineralogical characterizations of solid deposits collected from heat exchanger surfaces and of suspended matters in water collected from a cooling system presented in previous works. These studies showed that calcite is the main constituent (72–95% weight percent) followed by silica (0.3–12%) and illite (2.5–3%).

Fig. 3 presents scanning electron micrographs of the three types (silica, calcite, illite) of seed particles, enlarged 750 times. The specific surface area and particle size of each type of seed were previously measured by Laser Granulometry « in hydro method ». The calcite seeds shown are seen to have a roughly cubic shape with an average edge size of about 10 μm. Assuming that the edge length (a) of our seed calcite crystals is 10 μm, and knowing the density of calcite ($\rho_{calcite} = 2.71 \cdot 10^3$ kg·m$^{-3}$) and the mass introduced in the reactor ($m_s = 0.075$ g $= 7.5 \cdot 10^{-5}$ kg to obtain 100 mg·L$^{-1}$ for the total volume of working solution), we can calculate the total surface available for growth:

$$(S_{T\ calcite})\text{in m}^2 : \ \mathbf{S_{T\ calcite}} = 1.662 \cdot 10^{-2}\ \text{m}^2$$

The specific surface area of the calcite seeds ($S_{specific}$) in m$^2$·g$^{-1}$ is calculated as:

$$S_{sp} = \frac{S_T}{m_S} = \frac{1.662 \cdot 10^{-2}}{0.075} = 0.222\ \text{m}^2 \cdot \text{g}^{-1}$$

The calculated specific surface area of calcite seeds, 0.222 m$^2$·g$^{-1}$, corresponding to a cubic shape of 10 μm edge length is noticeably similar to that obtained by measurement (0.266 m$^2$·g$^{-1}$). This result is in agreement with values reported in a number of previous studies [32–35] (see Table 2A).

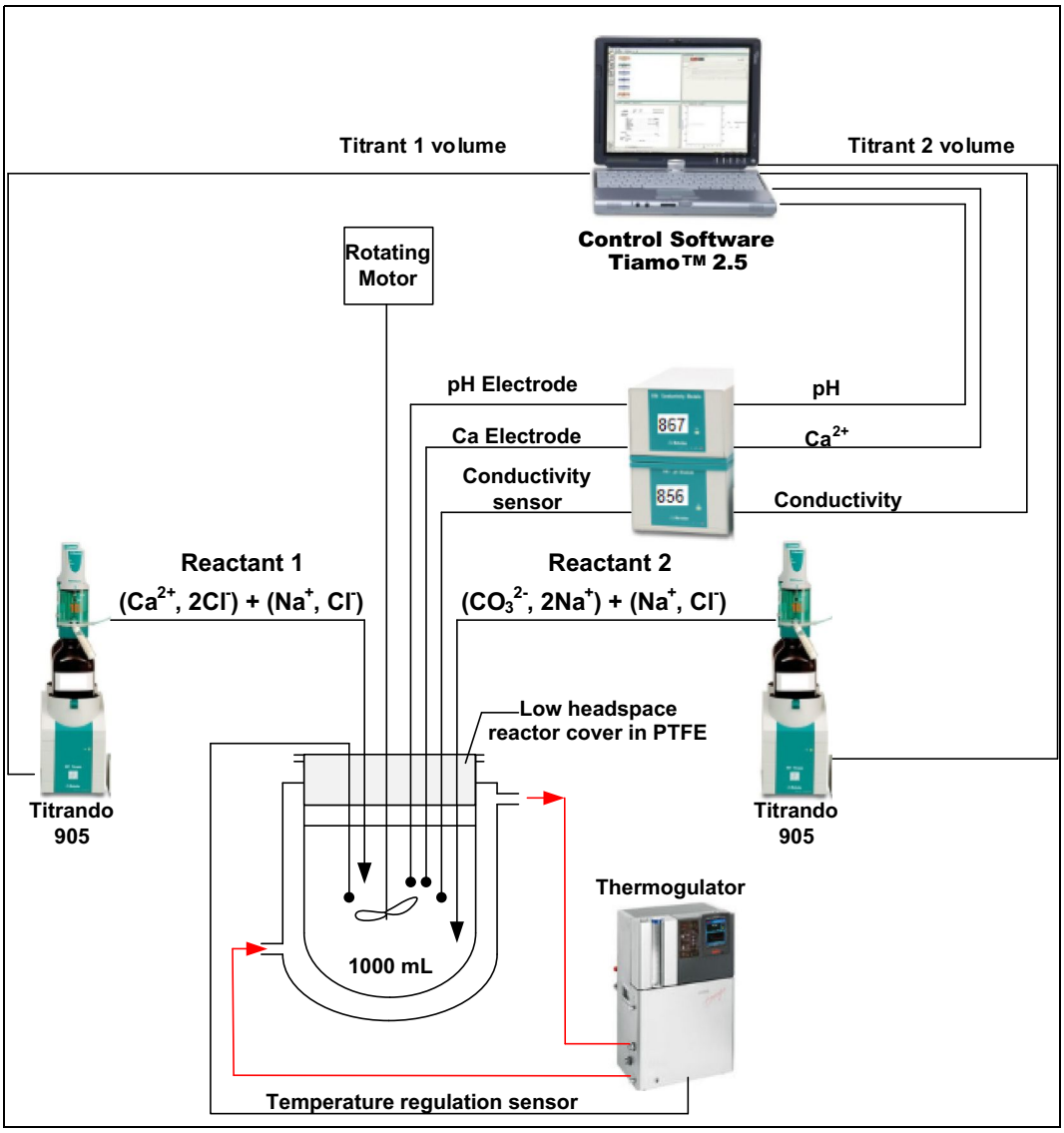


**Fig. 2.** Constant composition experimental setup.

Assuming that the edge length (a) of our silica and illite seed crystals is 10 μm, and knowing the densities of silica and illite ($\rho_{silica} = 2.22 \cdot 10^3$ kg·m$^{-3}$, $\rho_{illite} = 2.29 \cdot 10^3$ kg·m$^{-3}$), we can likewise calculate the total surface available for growth corresponding to each seed type: $\mathbf{S_{T\ silica}} = 2.028 \cdot 10^{-2}$ m$^2$ and $\mathbf{S_{T\ illite}} = 1.968 \cdot 10^{-2}$ m$^2$. The specific surface area calculations for the silica and illite seeds ($S_{specific}$) in m$^2$·g$^{-1}$ yield: $\mathbf{S_{Sp\ silica}} = 0.270$ m$^2 \cdot$ g$^{-1}$ and $\mathbf{S_{Sp\ illite}} = 0.262$ m$^2 \cdot$ g$^{-1}$. The results of these calculations and the corresponding measurements are reported in Table 2B.

Several inhibitors of carbonate mineral scale are proposed in the literature. They include polyphosphates [36–38,32,39], phosphonates [36,40] and synthetic polymeric inhibitors such as polyacrylic acids [41,42], polycarboxylic acids [43,44], polymaleic acids [45,46], polyaspartic acids [47,48] and copolymers containing acrylic, carboxylic, maleic functional groups [49–51]. Inhibitor effectiveness depends on numerous factors, including functional group [52], polymer concentration [36], molecular weight [53,52] and temperature [36].

Among the many inhibitor studies reported in the literature, few were conducted with the citric additive molecule as inhibitor of calcium carbonate growth. There are three carboxylic functional groups in a citrate molecule (see Table 2C). The citrate molecule is used in many areas such as food, cosmetics (soaps, shower gels, shampoos, etc.) and is also used as a natural household product for purposes such as limestone prevention and as an antioxidant. It was used as additive in this study. In order to compare the effects of number of carboxylic functional groups and molecular mass on the efficiency of calcite growth inhibition, a copolycarboxylic additive containing a greater number of carboxylic functional groups was chosen as the second additive.

## 4. Results and discussion

All experiments were conducted at supersaturation ratio $\Omega = 7.6$ and at pH = 8.5. The precipitation rates in the presence of seeds (with and without the presence of additives) were determined from plots of the volume of reactants added as a function of time, using the Tiamo 2.5 curve-fitting software. The rates of calcium carbonate formation, $R_m$, in mol·min$^{-1}$·m$^{-2}$ were calculated from the rate of addition of reactants (dV/dt) in L·min$^{-1}$, of concentration $C_T$ in mol·L$^{-1}$, normalized by the total surface area $A_t$ of seed crystals in m$^2$ [54]:

**Table 2**
Physico-chemical properties of the seed crystals and additives used in this study – (A) average particle size and specific surface area data reported in the literature and measured in our experiments; (B) measured and calculated values of specific surface area for the different types of seed crystal; (C) characteristics of the additives used in our experiments.

| Seed type | Literature | | Experimental seed crystal data measured by Laser granulometry (hydro method) | |
|---|---|---|---|---|
| | Average particle size (μm) | Specific surface area ($m^2 \cdot g^{-1}$) | Average particle size (μm) | Specific surface area ($m^2 \cdot g^{-1}$) |
| *(A)* | | | | |
| Silica | 0.18 | 21.5 [59] | 31 | 0.217 |
| | 1.5–15 | 0.83 ± 0.01 [60] | | |
| | | 0.053 [34] | | |
| | | 0.08 à 0.24 [61] | | |
| | 0.140 | 20 [62] | | |
| Calcite | | 0.278 [34] | 34.7 | 0.266 |
| | 10 | 0.22 [33] | | |
| | | 0.22 [32] | | |
| | 10–100 | 0.29 [35] | | |
| Illite | <2 | 7.3 à 12.3 [63] | 22.9 | 0.712 |
| | | 41 ± 3 [64] | | |

| Seed type | $S_T$ ($m^2$) | Measured $S_{sp}$ ($m^2 \cdot g^{-1}$) | Calculated $S_{sp}$ ($m^2 \cdot g^{-1}$) | $S_{sp\ measured}/S_{sp\ calculated}$ |
|---|---|---|---|---|
| *(B)* | | | | |
| Silica | $2.028 \cdot 10^{-2}$ | 0.217 | 0.270 | 0.80 |
| Calcite | $1.662 \cdot 10^{-2}$ | 0.266 | 0.222 | 1.20 |
| Illite | $1.968 \cdot 10^{-2}$ | 0.712 | 0.262 | 2.72 |

| Additive | Copolycarboxylic | Citrate (citric acid) |
|---|---|---|
| *(C)* | | |
| Developed formula | 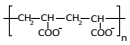 | 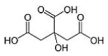 |
| | $n(C_6H_6O_4)$ | $(C_6H_8O_7)$ |
| Average molecular weight ($g \cdot mol^{-1}$) | 2000 | 192.12 |
| Density | 1.3 | 1.66 |
| pH at 25 °C | 4 | $pK_{a1} = 3.13$ $pK_{a2} = 4.76$ $pK_{a3} = 6.40$ |
| Active matter (%) | 55 | – |
| Viscosity at 25 °C (mPa·s) | 500 | – |

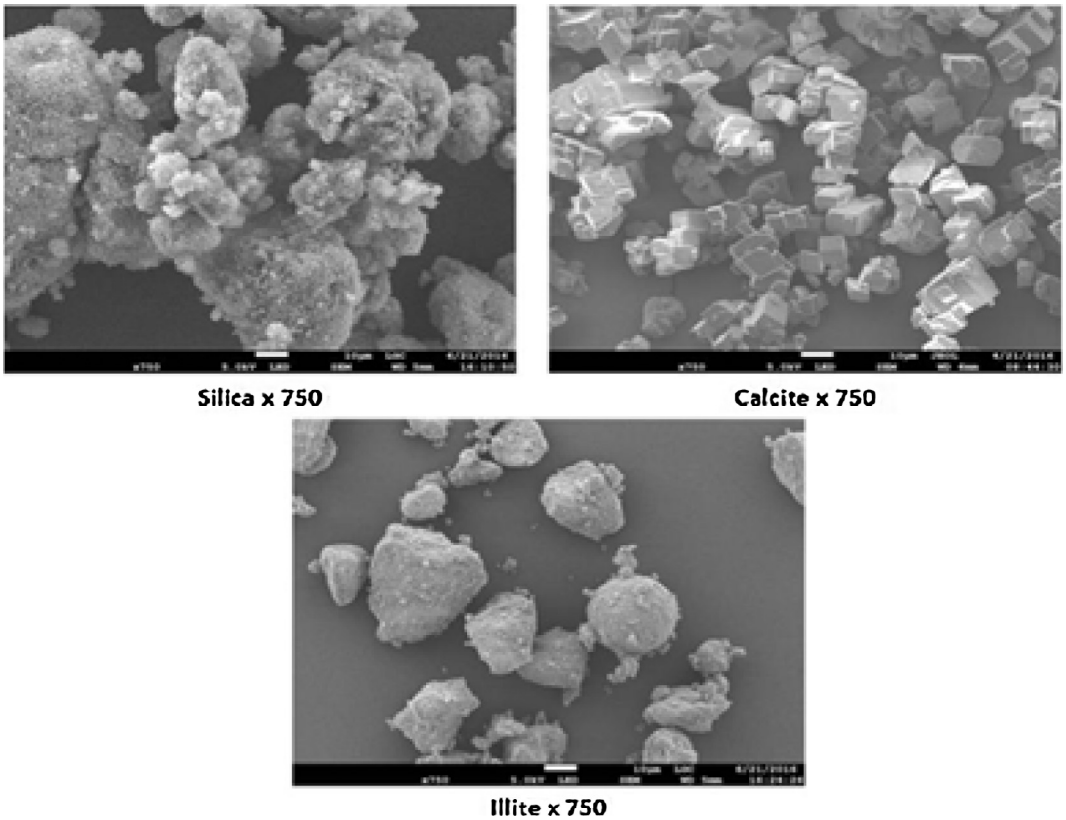


**Fig. 3.** Seed morphologies obtained by SEM.

$$R_m = \frac{dV}{dt}\frac{C_T}{A_t} \quad (19)$$

In our case, the total surface area $A_t$ used for $R_m$ calculation was obtained from the measured seed specific surface area values, reported in Table 2A.

The inhibition of the calcite crystals growth rate with additives, expressed as a percentage (%), is given by the following equation [54]:

$$\text{Inhibition rate } (\%) = 100 \times \left(1 - \frac{R_m}{R_0}\right) \quad (20)$$

where $R_0$ and $R_m$ are the calcite crystal growth rates corresponding respectively to the absence and the presence of inhibitor additives.

The influence of temperature on crystal growth rate is generally described by the Arrhenius formulation:

$$R_m = k e^{-\frac{E_a}{RT}} \quad (21)$$

where k is the pre-exponential factor, $E_a$ the activation energy in $kJ{\cdot}mol^{-1}$, R the universal gas constant ($R = 8.314\ J{\cdot}mol^{-1}{\cdot}K^{-1}$) and T the absolute temperature in Kelvin.

### *4.1. Effect of calcite seeds amount on the growth kinetics of $CaCO_3$ at 25 °C*

Experiments were performed in the absence or presence of calcite seeds at two different concentrations representative of those found in rivers ($10\ mg{\cdot}L^{-1}$ and $100\ mg{\cdot}L^{-1}$) under conditions of constant supersaturation and a solution temperature of 25 °C. Fig. 4A represents the reaction volume vs time curves for the three cases, illustrating the variation in volume of reactant solutions added into the solution over time. The experimental results are reported in Table 3.

In the absence of seeds, for a degree of supersaturation greater than 10 and at a temperature of 25 °C, a latent time for crystal growth of around 5 h is estimated using the formula reported by He et al. [55]. So, under our experimental conditions (supersaturation of 7.6 and at 25 °C), a latent time greater than 5 h could be expected as is characterized by the slope of the volume vs time curve of added calcium reactant solution remaining close to zero. The small deviation from zero value (without seeds) is due to the thin layer of calcite deposited with time, on the internal surface of the reactor, when the supersaturation solution is introduced, and has been taken into account in all the experiments, for growth rate calculation.

In the presence of seeds at low concentration ($10\ mg{\cdot}L^{-1}$), calcite crystal growth rate is higher than in the absence of seeds, with a value of $R_{m\ 10\ mg/L} = 5.36 \cdot 10^{-4}\ mol{\cdot}m^{-2}{\cdot}min^{-1}$. When the calcite seed concentration increases to $100\ mg{\cdot}L^{-1}$ (increase in the total surface area introduced), the crystal growth rate increases more significantly ($R_{m\ 100\ mg/L} = 6.29 \cdot 10^{-4}\ mol{\cdot}m^{-2}{\cdot}min^{-1}$) and is higher than for the $10\ mg{\cdot}L^{-1}$ concentration of calcite seeds. For the same degree of supersaturation, the increase in the amount of calcite seeds introduced into the reactor contributes to the increase in crystal growth rate. These results are in agreement with the work of Reddy who reported that the rate of crystallization varies

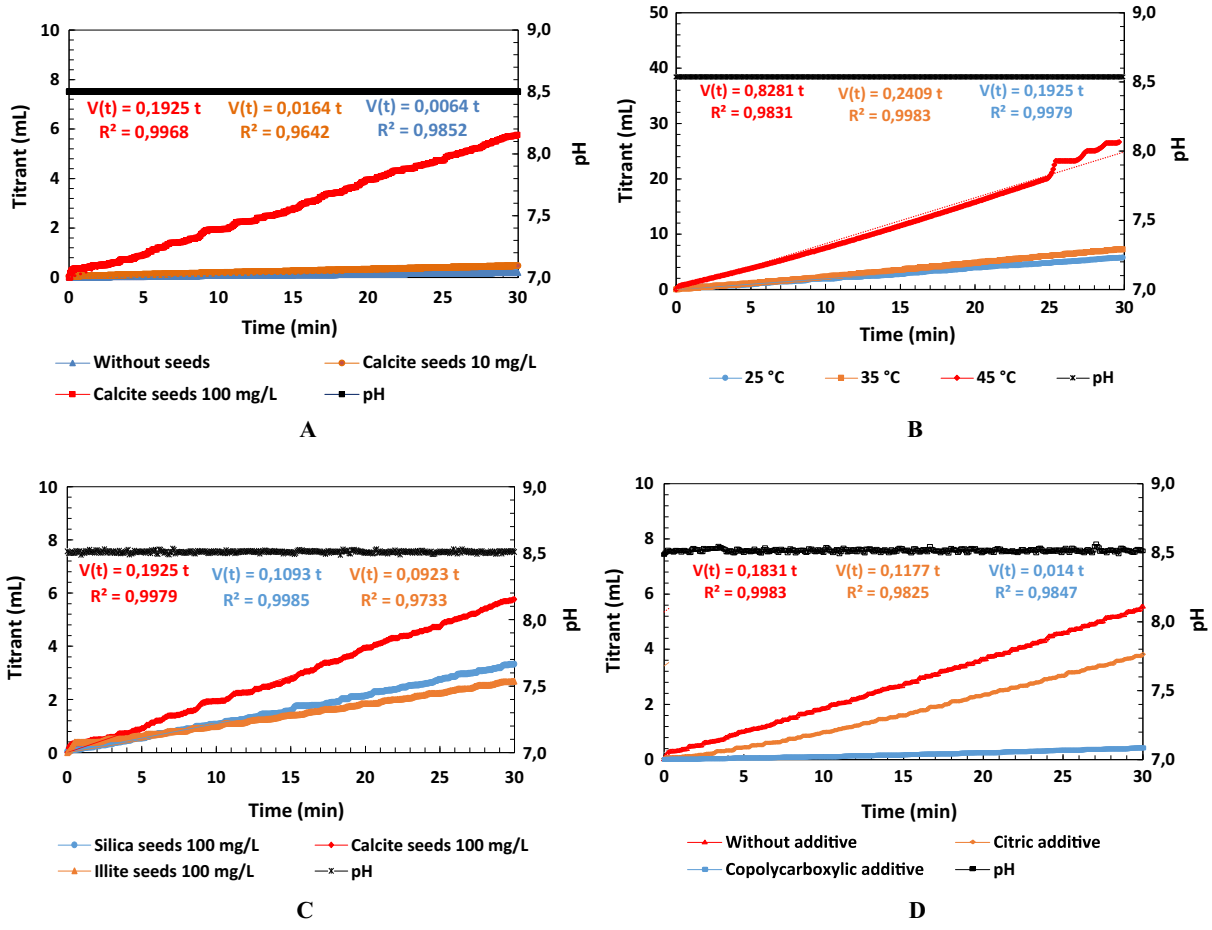


**Fig. 4.** Influence of different factors affecting calcite growth kinetics – (A) effect of calcite seeds amount on the growth kinetics of $CaCO_3$ at 25 °C; (B) effect of solution temperature on calcite growth rate at constant calcite seed concentration; (C) effect of seed type on calcite growth rate at constant seed concentration and (D) effect of inhibitors on calcite growth rate at 35 °C with a constant calcite seed concentration.

**Table 3**
Synthesis of crystal growth kinetic rate values under different experimental conditions.

| Supersaturation Ω = 7.6 | dV/dt (mL·min$^{-1}$) | $R_m$ (mol·m$^{-2}$·min$^{-1}$) | Inhibition rate (%) | $K_a$ Additive adsorption affinity constant (L·mol$^{-1}$) |
|---|---|---|---|---|
| *Effects of calcite seed quantity on the growth kinetics of $CaCO_3$ at 25 °C* | | | | |
| Without seed | 0.0064 | – | – | |
| Calcite seed 10 mg·L$^{-1}$ | 0.0164 | $5.36 \cdot 10^{-4}$ | – | |
| Calcite seed 100 mg·L$^{-1}$ | 0.1925 | $6.29 \cdot 10^{-4}$ | – | |
| *Effects of solution temperature on the calcite growth kinetics at constant calcite seed concentration (100 mg·L$^{-1}$)* | | | | |
| 25 °C | 0.1925 | $6.29 \cdot 10^{-4}$ | – | |
| 35 °C | 0.2409 | $7.88 \cdot 10^{-4}$ | – | |
| 45 °C | 0.8281 | $2.71 \cdot 10^{-3}$ | – | |
| *Effects of seed type on the calcite growth kinetics at 25 °C and at constant seed concentration (100 mg·L$^{-1}$)* | | | | |
| Calcite seed 100 mg·L$^{-1}$ | 0.1925 | $6.29 \cdot 10^{-4}$ | – | |
| Silica seed 100 mg·L$^{-1}$ | 0.1093 | $4.38 \cdot 10^{-4}$ | – | |
| Illite seed 100 mg·L$^{-1}$ | 0.0923 | $1.13 \cdot 10^{-4}$ | – | |
| *Effects of inhibitor additives on calcite growth kinetics at 35 °C and constant calcite seed concentration (100 mg·L$^{-1}$)* | | | | |
| Without additive | 0.1831 | $6.27 \cdot 10^{-4}$ | – | – |
| Citric additive | 0.1177 | $3.85 \cdot 10^{-4}$ | 38.6 | $2.4 \cdot 10^{5}$ |
| Copolycarboxylic additive (PC) | 0.0140 | $4.58 \cdot 10^{-5}$ | 92.7 | $5.1 \cdot 10^{7}$ |
| *Effect of temperature on the additive effectiveness at constant calcite seed concentration (100 mg·L$^{-1}$)* | | | | |
| Citrate | 25 °C | 0.1115 | $3.65 \cdot 10^{-4}$ | 43.2 | $2.8 \cdot 10^{5}$ |
| | 35 °C | 0.1514 | $4.95 \cdot 10^{-4}$ | 37.6 | $2.3 \cdot 10^{5}$ |
| | 45 °C | 0.6052 | $1.98 \cdot 10^{-3}$ | 26.9 | $1.4 \cdot 10^{5}$ |
| Copolycarboxylate (PC) | 25 °C | 0.0026 | $8.50 \cdot 10^{-6}$ | 98.6 | $2.9 \cdot 10^{8}$ |
| | 35 °C | 0.0130 | $4.25 \cdot 10^{-5}$ | 94.6 | $7.0 \cdot 10^{7}$ |
| | 45 °C | 0.0451 | $1.48 \cdot 10^{-4}$ | 94.4 | $6.9 \cdot 10^{7}$ |

depending on the amount of seed added into the working solution [37]. But in our case, no interpretation can be done on growth mechanism because, for the smallest quantity of seeds (10 mg·L$^{-1}$) the limit of the method is probably reached. Given the high level of supersaturation used, we cannot guarantee that secondary nucleation does not occur. It is why, in the following sections all the experiments will be performed with 100 mg·L$^{-1}$.

However, the results show that, considering that the concentration of calcite particles in river water can reach sometimes 300 mg·L$^{-1}$, this has serious implications for industrial or power plant cooling systems. A particle concentration of this magnitude in cooling would lead to a substantial increase in the growth rate of calcite crystals and, in turn, cause a dramatic increase in the rate of scale deposition and build-up on heat exchanger surfaces.

### 4.2. Effect of solution temperature on calcite growth rate at constant calcite seed concentration

Constant composition experiments were carried out at three different temperatures (25 °C, 35 °C and 45 °C) for a supersaturated solution (Ω = 7.6) and a constant concentration of calcite seeds (100 mg·L$^{-1}$). As can be seen from Fig. 4B, the crystal growth rate differed slightly between 25 °C and 35 °C ($R_{m\ 25\ °C} = 6.29 \cdot 10^{-4}$ mol·m$^{-2}$·min$^{-1}$, $R_{m\ 35\ °C} = 7.88 \cdot 10^{-4}$ mol·m$^{-2}$·min$^{-1}$) whereas at 45 °C there was a pronounced difference, with a progressively faster growth rate observed ($R_{m\ 45\ °C} = 2.71 \cdot 10^{-3}$ mol·m$^{-2}$·min$^{-1}$ (see Table 3).

The experimental determination of the activation energy term $E_a$ in Eq. (21) is obtained by plotting Ln $R_m$ as a function of 1/RT. The value of 56.3 kJ·mol$^{-1}$ obtained under our experimental conditions is in agreement with the $E_a$ values of calcite crystallization reported in the literature, which range from 45 ± 4 kJ·mol$^{-1}$ [33] to 66 ± 2 kJ·mol$^{-1}$ [56]. This range of activation energies suggests that the rate-determining step is either the adsorption onto the crystal surface or integration into the crystal lattice.

Given that the coolant temperature fluctuates from the inlet side (25 °C) to the outlet side (45 °C) of cooling systems, the calcite growth rate could vary according, increasing the probability of more substantial deposition towards the end of the flow circuit.

### 4.3. Effect of seed type on calcite growth rate at constant seed concentration

The presence of many different types of particles in river water used in the cooling system may contribute to the fouling on heat exchange surfaces in contact with circulating water.

The experiments were performed using three types of seeds at 100 mg·L$^{-1}$ (calcite, illite and silica), the characteristics of which are reported in Table 2A. The temperature of the supersaturated solution was maintained at 25 °C for all tests.

Fig. 4C shows that a faster rate of calcium carbonate crystal growth occurs in the presence of calcite seeds ($R_{m\ calcite} = 6.29 \cdot 10^{-4}$ mol·m$^{-2}$·min$^{-1}$) than in the presence of the other seeds ($R_{m\ silica} = 4.38 \cdot 10^{-4}$ mol·m$^{-2}$·min$^{-1}$, $R_{m\ illite} = 1.13 \cdot 10^{-4}$ mol·m$^{-2}$·min$^{-1}$). The rate of crystal growth on the illite seeds is lower than on the other seeds although it has the greatest surface area. The very high reactivity of the calcite seeds observed under the experimental conditions is consistent with the results of the mineralogical characterization.

### 4.4. Effect of inhibitors on calcite growth rate at 35 °C with constant calcite seed concentration

To prevent fouling, additives (acids, stoichiometric additives, threshold inhibition additives, polymeric additives) are often injected into the water in cooling circuits. The use of acids and stoichiometric-effect additives like EDTA or citrate is limited due to their impact on the aquatic environment as well as for economic reasons (cost-effectiveness ratio). The polymeric additives such as polycarboxylic additives are increasingly used in many industries.

Tests were conducted with two different additives, one of which is a citric additive and the other a copolycarboxylic additive (PC). The characteristics of these additives are presented in Table 2B. These tests were carried out in a supersaturated solution

($\Omega$ = 7.6) at a constant temperature of 35 °C and a constant calcite seed concentration (100 mg·L$^{-1}$).

The experimental results are shown in Fig. 4D. The calcium carbonate growth rate in the absence of additive is characterized as high, with a growth rate of 6.27 · 10$^{-4}$ mol·m$^{-2}$·min$^{-1}$. In presence of the citric additive, the rate of calcium carbonate growth is reduced to 3.85 · 10$^{-4}$ mol·m$^{-2}$·min$^{-1}$, corresponding to a 38.6% of inhibition rate. By contrast, when copolycarboxylic inhibitor is used as the additive under the same experimental conditions, the calcite growth rate is drastically reduced to 4.58 · 10$^{-5}$ mol·m$^{-2}$·min$^{-1}$ with an inhibition rate estimated at 92.7% (see Table 3).

For an equivalent concentration of active matter (0.5 mg·L$^{-1}$), the copolycarboxylate additive exhibits higher efficiency in terms of calcite crystal growth inhibition in these experimental conditions. The first explanation could be that the difference in efficiency between these two additives is due to their different modes of action on crystal growth: the citrate additive complexes the calcium ions in the bulk solution leaving less calcium available for growth on the active sites of seeds whereas the copolycarboxylate additive acts by surface adsorption, blocking active growth sites on the seed surface and preventing further crystal growth. Furthermore, it is generally recognized that the inhibitory effect of polymeric additives on calcium carbonate crystal formation is influenced by both the location of the adsorbed inhibitor molecules at the crystals surface and the extent of chemical bonding with the surface. Therefore, the greater the number of carboxyl groups contained in each molecule of copolycarboxylic additive, the stronger its surface-binding capacity and the higher is the inhibitory effect under identical conditions [49].

### *4.5. Effects of temperature on additive efficiency at constant calcite seeds concentration*

All experiments were performed at three different temperatures in order to cover the range of temperatures commonly encountered in cooling circuits. Tests were run for each of the two additives (citric and copolycarboxylic additives), with all other experimental conditions (degree of supersaturation, additive concentration, 100 mg·L$^{-1}$ calcite seed concentration) remaining the same. The experimental results are shown in Fig. 5 and the crystal growth rate values for these experiments are provided in Table 3. It should be noted that the crystal growth rate increases with the working solution temperature while the inhibition rate, on the contrary, decreases with increasing solution temperature regardless of the type of additive used. Both tendencies are in agreement with those observed in pilot plant experiments [1].

The increase in growth rate with temperature suggests that the reaction follows the Arrhenius law and may be characterized by a change in the activation energy owing to the presence of additives.

The activation energies obtained under these experimental conditions are, respectively, 66.2 kJ·mol$^{-1}$ for citric additive and 96.4 kJ·mol$^{-1}$ for the copolycarboxylic additive. Comparing these values to the activation energy obtained during the experiment without additives (56.3 kJ·mol$^{-1}$), the increase in activation energies provides an explanation for the inhibition effectiveness of calcite crystal growth.

For many sparingly soluble salts, the mechanism of crystal growth rate inhibition can be described as an adsorption of active molecules at crystal growth sites on the mineral surfaces. The adsorption process can often be interpreted in terms of a Langmuir-type isotherm represented by the following equation [57]:

$$\frac{R_0}{R_0 - R} = 1 + \frac{1}{K_a C_{additive}} \tag{22}$$

where R and $R_0$ are the respective rates of crystal growth in the presence and absence of inhibitors.

$K_a$ is the affinity constant of the substrate for the inhibitor ion and $C_{additive}$ is the inhibitor concentration.

The $K_a$ values for the citric and copolycarboxylic additives, corresponding to the different experiments, are reported in Table 3.

The value of the affinity constant calculated from our experiments in the presence of citric additive ranged from 1.4 · 10$^5$ (45 °C) to 2.8 · 10$^5$ at 25 °C. Under similar experimental conditions ($\Omega$ = 4.5, pH = 8.55 ± 0.02, temperature of 25 °C), Reddy et al. [43] found affinity constant values ranging from 0.61 to 0.88 · 10$^5$ at a citric additive concentration of 1 mg·L$^{-1}$ whereas in our experimental conditions, the affinity constant is 2.8 · 10$^5$ at 25 °C with an additive concentration of 0.5 mg·L$^{-1}$ of citrate. This difference is probably related to the amount of calcite seed used.

The corresponding values for copolycarboxylic additive, calculated under our experimental conditions, are in the 5.1 · 10$^7$ to 2.9 · 10$^8$ range (see Table 3). However, we are unable to compare these results with published data as there is nothing in the literature, to our knowledge, reporting affinity constants for copolycarboxylic additive.

It should be noted that the affinity constant values for the citric additive are significantly lower, by a 100 to a 1000 times, than the

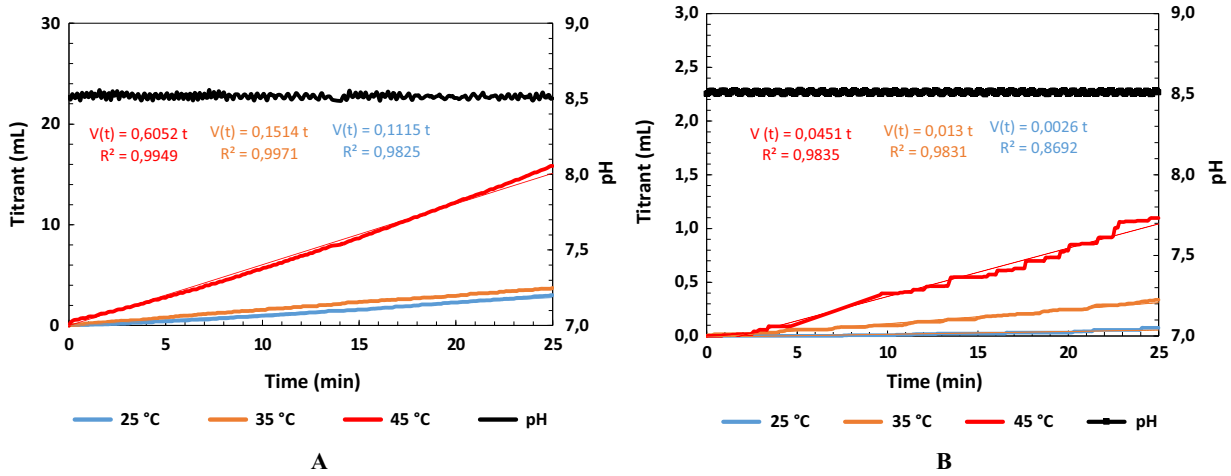


**Fig. 5.** Effect of temperature on additive efficiency at constant calcite seed concentration – (A) citric additive at 0.5 mg·L$^{-1}$ in the presence of 100 mg·L$^{-1}$ of calcite seeds – (B) copolycarboxylic additive at 0.5 mg·L$^{-1}$ in the presence of 100 mg·L$^{-1}$ of calcite seeds.

values obtained with the copolycarboxylic additive. This significant difference is a key factor in the relative effectiveness of these two additives in calcite growth inhibition. Finally, the impacts of both additives can be analyzed assuming a common adsorption phenomena modulated by the abundance of carboxylic functional group in the additive.

Moreover, for both additives, the affinity constant decreases with increasing temperature. This observation suggests adsorption of the additive molecules on the active growth sites of the calcite seed crystals.

## 5. Conclusion

This study provides comprehensive knowledge of the relative contribution of different components of suspended particulate matter naturally present in recirculating cooling water to calcite growth kinetics and the efficiency of two additive inhibitors in blocking or retarding the growth steps, using the constant composition method at constant supersaturation.

Fluctuations in the amount or concentration of suspended particulate matter in industrial cooling systems can lead to a substantial increase in calcite crystal growth rates and consequently to a drastic increase in fouling or mineral scale on heat exchanger surfaces.

Given the temperature fluctuations that occur in recirculating cooling systems from the inlet section (25 °C) to the outlet section (45 °C), the calcite growth rate can potentially vary along the water passage with the likelihood of higher deposition rates and buildup towards the end of the circuit.

Of the three particles used (calcite, silica, illite), representative of the main components of suspended solids in circulating cooling water, the calcite particles have greater reactivity than silica and illite particles in terms of the crystal growth kinetics of crystal growth of calcium carbonate. The reactivity of calcite particles observed under our experimental conditions is consistent with the results of the mineralogical analyses performed in industrial systems.

Despite the presence of the same carboxylic functional groups in the two additives tested, the copolycarboxylic additive has a higher inhibition efficiency against calcium carbonate crystal growth than the citric additive. This difference can be explained by the presence of a larger number of carboxylic functional groups in the copolycarboxylic additive molecule.

It should be noted that, regardless of the type of additive used, the crystal growth rate increases with the working solution temperature whereas the inhibition rate decreases with increased solution temperatures. This last tendency is in agreement with the trend observed in pilot plant experiments [1].

## References


[1] Th. Neveux, M. Bretaud, N. Chhim, K. Shakourzadeh, S. Rapenne, Pilot plant experiments and modeling of $CaCO_3$ growth inhibition by the use of antiscalant polymers in recirculating cooling circuits, Desalination 397 (2016) 43–52.

[2] Kh. Rahmani, R. Jadidian, S. Haghtalab, Evaluation of inhibitors and biocides on the corrosion, scaling and biofouling control of carbon steel and copper-nickel alloys in a power plant cooling water system, Desalination 393 (2015) 174–185.

[3] Ali A. Al-Hamzah, Christopher M. Fellows, A comparative study of novel scale inhibitors with commercial scale inhibitors used in seawater desalination, Desalination 359 (2015) 22–25.

[4] S. Phuntsho, F. Lotfi, S. Hong, D.L. Shaffer, M. Elimelech, H.K. Shon, Membrane scaling and flux decline during fertiliser-drawn forward osmosis desalination of brackish, Water Res. 57 (2014) 172–182.

[5] A. Al-Rawajfeh, Simultaneous desorption-crystallization of $CO_2$-$CaCO_3$ in multi stage flash (MSF) distillers, Chem. Eng. Process.: Process. Intensif. 47 (2008) 2262–2269.

[6] S. Ghani, Noura S. Al-Deffeeri, Impacts of different antiscalant dosing rates and their thermal performance in Multi Stage Flash (MSF) distiller in Kuwait, Desalination 250 (2010) 463–472.

[7] Heming Luo, Dejun Chen, Xiaoping Yang, Xia Zhao, Huixia Feng, Mingyang Li, Junqiang Wang, Synthesis and performance of a polymeric scale inhibitor for oilfield application, J. Petrol. Explor. Prod. Technol. 5 (2015) 177–187.

[8] M. Chaussemier, E. Pourmohtasham, D. Gelus, N. Pécoul, H. Perrot, J. Lédion, H. Cheap-Charpentier, O. Horner, State of art of natural inhibitors of calcium carbonate scaling. A review article, Desalination 356 (2015) 47–55.

[9] O.S. Pokrovsky, Precipitation of calcium and magnesium carbonates from homogeneous supersaturated solutions, J. Cryst. Growth 186 (1998) 233–239.

[10] E. Ruiz-Agudo, C.V. Putnis, C. Rodriguez-Navarro, A. Putnis, Effect of pH on calcite growth at constant $aCa^{2+}/aCO_3^{2-}$ ratio and supersaturation, Geochim. Cosmochim. Acta 75 (1) (2011) 284–296.

[11] W.-C. Chien, C.-C. Lee, C.Y. Tai, Heterogeneous nucleation rate of calcium carbonate derived from induction period, Ind. Eng. Chem. Res. 46 (2007) 6435–6441.

[12] C.H. van der Weijden, R.D. van der Weijden, Calcite growth: rate dependence on saturation, on ratios of dissolved calcium and (bi)carbonate and on their complexes, J. Cryst. Growth 394 (2014) 137–144.

[13] C.Y. Tai, W.C. Chien, Interpreting the effects of operating variables on the induction period of $CaCl_2$–$Na_2CO_3$ system by a cluster coagulation model, Chem. Eng. Sci. 58 (2003) 3233–3241.

[14] E.D. Zanotto, M.C. Weinberg, Saturation effects in homogeneous and heterogeneous crystal nucleation, J. Non-Cryst. Solids 105 (1988) 53–62.

[15] Branka Njegic-Dzakula, Giuseppe Falini, Ljerka Brecevic, Zeljko Skoko, Damir Kralj, Effects of initial supersaturation on spontaneous precipitation of calcium carbonate in the presence of charged poly-L-amino acids, J. Colloid Interf. Sci. 343 (2010) 553–563.

[16] Yi-Pin Lin, P.C. Singer, Effects of seed material and solution composition on calcite precipitation, Geochim. Cosmochim. Acta 69 (118) (2005) 4495–4504.

[17] J. Gomez-Morales, J. Torrent-Burgués, A. Lopez-Macipe, Precipitation of calcium carbonate from solutions with varying $Ca^{2+}$/carbonate ratios, J. Cryst. Growth 166 (1996) 1020–1026.

[18] E. Ruiz-Agudo, C.V. Putnis, C. Rodriguez-Navarro, A. Putnis, Effect of pH on calcite growth at constant $aCa^{2+}/aCO_3^{2-}$ ratio and supersaturation, Geochim. Cosmochim. Acta 75 (2011) 284–296.

[19] J.D. Rodriguez-Blanco, S. Shaw, P. Bots, T. Roncal-Herrero, L.G. Benning, The role of pH and Mg on the stability and crystallization of amorphous calcium carbonate, J. Alloys Compd. 536 (2012) S477–S479.

[20] Tung A. Hoang, H. Ming Ang, Andrew L. Rohl, Effects of temperature on the scaling of calcium sulphate in pipes, Powder Technol. 179 (2007) 31–37.

[21] Maria G. Lioliou, Christakis A. Paraskeva, Petros G. Koutsoukos, Alkiviades C. Payatakes, Heterogeneous nucleation and growth of calcium carbonate on calcite and quartz, J. Colloid Interf. Sci. 308 (2007) 421–428.

[22] G.J. Stockmann, D. Wolff-Boenisch, N. Bovet, S.R. Gislason, E.H. Oelkers, The role of silicate surfaces on calcite precipitation kinetics, Geochim. Cosmochim. Acta 135 (2014) 231–250.

[23] R. Isopescua, C. Mateescu, M. Mihai, G. Dabija, The effects of organic additives on induction time and characteristics of precipitated calcium carbonate, Chem. Eng. Res. Des. 88 (2010) 1450–1454.

[24] M.M. Reddy, Calcite growth-rate inhibition by fulvic acid and magnesium ion—possible influence on biogenic calcite formation, J. Cryst. Growth 352 (2012) 151–154.

[25] J.M. Astilleros, L. Fernández-Díaz, A. Putnis, The role of magnesium in the growth of calcite: an AFM study, Chem. Geol. 271 (2010) 52–58.

[26] A. Niedermayr, S.J. Köhler, M. Dietzel, Impacts of aqueous carbonate accumulation rate, magnesium and polyaspartic acid on calcium carbonate formation (6–40 °C), Chem. Geol. 340 (2013) 105–120.

[27] S. Ghizellaoui, M. Euvrard, J. Ledion, A. Chibani, Inhibition of scaling in the presence of copper and zinc by various chemical processes, Desalination 206 (2007) 185–197.

[28] S. Ghizellaoui, M. Euvrard, Assessing the effect of zinc on the crystallization of calcium carbonate, Desalination 220 (2008) 394–402.

[29] R. Beck, M. Seiersten, J.-P. Andreassen, The constant composition method for crystallization of calcium carbonate at constant supersaturation, J. Cryst. Growth 380 (2013) 187–196.

[30] L.N. Plummer, E. Busenberg, The solubilities of calcite, aragonite and vaterite in $CO_2$-$H_2O$ solution between 0 and 90 °C, and an evaluation of the aqueous model for the system $CaCO_3$-$CO_2$-$H_2O$, Geochim. Cosmochim. Acta 46 (116) (1982) 1011–1040.

[31] David L. Parkhurst, User's guide to PHREEQC: a computer program for speciation, reaction-path, advective-transport and inverse geochemical calculations, Lakewood, Colorado, 1995.

[32] W.A. House, Inhibition of calcite crystal growth by inorganic phosphate, J. Colloid Interf. Sci. 119 (1987) 505–511.

[33] Katrin I. Parsiegla, Joseph L. Katz, Calcite growth inhibition by copper (II) I. Effect of supersaturation, J. Cryst. Growth 200 (1999) 213–226.

[34] Y.-P. Lin, P.C. Singer, Effects of seed material and solution composition on calcite precipitation, Geochim. Cosmochim. Acta 69 (118) (2005) 4495–4504.

[35] R.D. Van der Weijden, A.E. van der Heijden, G.J. Witkamp, G.M. van Rosmalen, The influence of total calcium and total carbonate on the growth rate of calcite, J. Cryst. Growth 171 (1997) 190–196.

[36] R. Ketrane, B. Saidani, O. Gil, L. Leleyter, F. Baraud, Efficiency of five scale inhibitors on calcium carbonate precipitation from hard water: effect of temperature and concentration, Desalination 249 (2009) 1397–1404.

[37] M.M. Reddy, Crystallization of calcium carbonate in the presence of trace concentrations of phosphorus-containing anions, J. Cryst. Growth 41 (1977) 287–295.
[38] Y.-P. Lin, P.C. Singer, Inhibition of calcite precipitation by orthophosphate: speciation and thermodynamic considerations, Geochim. Cosmochim. Acta 70 (2006) 2530–2539.
[39] Y.-P. Lin, P.C. Singer, Inhibition of calcite crystal growth by polyphosphates, Water Res. 39 (2005) 4835–4843.
[40] N. Abdel-Aal, K. Sawada, Inhibition of adhesion and precipitation of $CaCO_3$ by aminopolyphosphonate, J. Cryst. Growth 256 (2003) 188–200.
[41] Q. Liu, Q. Wang, L. Xiang, Influence of poly acrylic acid on the dispersion of calcite nano-particles, Appl. Surf. Sci. 254 (2008) 7104–7108.
[42] J. Yu, M. Lei, B. Cheng, X. Zhao, Effects of PAA additive and temperature on morphology of calcium carbonate particles, J. Solid State Chem. 177 (2004) 681–689.
[43] M.M. Reddy, A.R. Hoch, Calcite crystal growth rate inhibition by polycarboxylic acids, J. Colloid Interf. Sci. 235 (2001) 365–370.
[44] E. Dousi, J. Kallitsis, A. Chrissanthopoulos, A.H. Mangood, E. Dalas, Calcite overgrowth on carboxylated polymers, J. Cryst. Growth 253 (2003) 496–503.
[45] Z. Shen, J. Li, K. Xu, L. Ding, H. Ren, The effect of synthesized hydrolyzed polymaleic anhydride (HPMA) on the crystal of calcium carbonate, Desalination 284 (2012) 238–244.
[46] Z. Amjad, P.G. Koutsoukos, Evaluation of maleic acid based polymers as scale inhibitors and dispersants for industrial water applications, Desalination 335 (2014) 55–63.
[47] J. Chen, L. Xu, J. Han, M. Su, Q. Wu, Synthesis of modified polyaspartic acid and evaluation of its scale inhibition and dispersion capacity, Desalination 358 (2015) 42–48.
[48] Y. Gao, L. Fan, L. Ward, Z. Liu, Synthesis of polyaspartic acid derivative and evaluation of its corrosion and scale inhibition performance in sea water utilization, Desalination 365 (2015) 220–226.
[49] L. Lei, Y. Zhou, J. Huang, Q. Yao, G. Liu, P. Zhang, W. Sun, W. Wu, Carboxylate-terminated double-hydrophilic block copolymer as an effective and environmental inhibitor in cooling water systems, Desalination 304 (2012) 33–40.
[50] M. Dietzsch, M. Barz, T. Schüler, S. Klassen, M. Schreiber, M. Susewind, N. Loges, M. Lang, N. Hellmann, M. Fritz, K. Fischer, P. Theato, A. Kühnle, M. Schmidt, R. Zentel, W. Tremel, PAA-PAMPS copolymers as an efficient tool to control $CaCO_3$ scale formation, Langmuir 29 (2013) 3080–3088.
[51] I.M. Pelin, Irina Popescu, D.M. Suflet, M. Aflori, V. Bulacovschi, Influence of maleic acid copolymers on calcium orthophosphates crystallization at low temperature, J. Cryst. Growth 377 (2013) 127–135.
[52] Ali A. Al-Hamzah, C.P. East, W.O.S. Doherty, C.M. Fellows, Inhibition of homogenous formation of calcium carbonate by poly(acrylic acid). The effect of molar mass and end-group functionality, Desalination 338 (2014) 93–105.
[53] A. Jada, R. Ait Akbour, C. Jacquemet, J.M. Suau, O. Guerret, Effect of sodium polyacrylate molecular weight on the crystallogenesis of calcium carbonate, J. Cryst. Growth 306 (2007) 373–382.
[54] Pavlos G. Klepetsanis, A. Kladi, T. Ostvold, C.G. Kontoyiannis, P.G. Koutsoukos, Z. Amjad, M.M. Reddy, The inhibition of calcium carbonate formation in aqueous supersaturated solutions, spontaneous precipitation and seeded crystal growth, Adv. Cryst. Growth Inhibition Technol. (2000) 123–128.
[55] S. He, A.T. Kan, M.B. Tomson, Inhibition of calcium carbonate precipitation in NaCl brines from 25–90 °C, Appl. Geochem. 14 (1999) 17–25.
[56] J.D. Rodriguez Blanco, S. Shaw, L.G. Benning, The kinetics and mechanisms of amorphous calcium carbonate (ACC) crystallization to calcite, via vaterite, Nanoscale 3 (2011) 265.
[57] P.G. Klepetsanis, P. Koutsoukos, G.-C. Chitanu, A. Carpov, The inhibition of calcium carbonate formation by copolymers containing maleic acid, in: Z. Amjad (Ed.), Water Soluble Polymers, Plenum Press, New York, 2002, pp. 117–129.
[58] D.R. Lide, Handbook of Chemistry and Physics, 72nd ed., CRC Press Inc., 1991–1992.
[59] Y. Qing, Z. Zenan, K. Deyu, C. Rongshen, Influence of nano-$SiO_2$ addition on properties of hardened cement paste as compared with silica fume, Constr. Build. Mater. 21 (2007) 539–545.
[60] L. Clausen, I. Fabricius, L. Madsen, Adsorption of pesticides onto quartz, calcite, kaolinite, and a-alumina, J. Environ. Qual. 30 (2001) 846–857.
[61] J. Plank, C. Schroefl, M. Gruber, M. Lesti, R. Sieber, Effectiveness of polycarboxylate superplasticizers in ultra-high strength concrete: the importance of PCE compatibility with silica fume, J. Adv. Concr. Technol. 7 (11) (2009) 5–12.
[62] S. Schwarz, K. Lunkwitz, B. Keßler, U. Spiegler, E. Killmann, W. Jaeger, Adsorption and stability of colloidal silica, Colloids Surf. A: Physicochem. Eng. Asp. 163 (2000) 17–27.
[63] S. Zhang, J.J. Sheng, Z. Qiu, Water adsorption on kaolinite and illite after polyamine adsorption, J. Petrol. Sci. Eng. 142 (2016) 13–20.
[64] F. Macht, K. Eusterhues, G.J. Pronk, K.U. Totsche, Specific surface area of clay minerals: comparison between atomic force microscopy measurements and bulk-gas ($N_2$) and -liquid (EGME) adsorption methods, Appl. Clay Sci. 53 (2011) 20–26.